Ceramics International 42 (2016) 11248–11255

Contents lists available at ScienceDirect

Ceramics International

journal homepage: www.elsevier.com/locate/ceramint

Inhibited grain growth in hydroxyapatite–graphene nanocomposites during high temperature treatment and their enhanced mechanical properties

Yi Liu [a], Jing Huang [a], Mitsuo Niinomi [b], Hua Li [a,*]

[a] Key Laboratory of Marine Materials and Related Technologies, Key Laboratory of Marine Materials and Protective Technologies of Zhejiang Province, Ningbo Institute of Materials Technology and Engineering, Chinese Academy of Sciences, Ningbo 315201, China
[b] Department of Biomaterial Science, Institute for Materials Research, Tohoku University, 2-1-1, Katahira, Aoba-ku, Sendai 980-8577, Japan

ARTICLE INFO

Article history:
Received 13 February 2016
Received in revised form
20 March 2016
Accepted 8 April 2016
Available online 9 April 2016

Keywords:
Ceramic matrix composites
Annealing
Interfaces
Grain growth
Hydroxyapatite
Graphene nanosheet

ABSTRACT

Nanostructured hydroxyapatite (HA)–graphene nanosheet (GN) composites have been fabricated by spark plasma sintering consolidation. Nanostructual evolution of the bioceramic-based composites during further high temperature heat treatment is characterized and enhanced mechanical strength is assessed. GN keeps intact after the treatment and its presence at HA grain boundaries effectively inhibits HA grain growth by impeding interconnection of individual HA grains. Microstructural characterization discloses strong coherent interfaces between GN and the (300) plane of HA crystals. This particular matching state in the composites agrees well with the competitive theoretical pull-out energy for single graphene sheet being departed from HA matrix. The toughening regimes that operate in HA–GN composites at high temperatures give clear insight into potential applications of GN for ceramic matrix composites.

1. Introduction

As one of the most popular bioceramics, hydroxyapatite (HA) has been extensively employed for biomedical applications. Yet, regardless of the successful application of HA in orthopedic surgery for promoting fast fixation of bony tissues, there are still concerns related to its long-term performances, i.e., intrinsic brittleness and low fracture toughness of HA. Tremendous efforts have therefore been made in past decades towards improving its strength and toughness by adding a second phase for load-bearing applications [1–5]. In general, composite materials have a structure comprising two or more components that differ in physical and chemical properties which have been combined to provide specific characteristics for particular applications. Enhancing stiffness and strength and precise property matching are always the predominant concerns in design and processing of the ceramic matrix composites. The discovery of graphene and its derivatives has sparked considerable interests in their use as reinforcements in various matrix materials to impart stiffness, strength, and toughness [6,7]. The 2D nature of graphene also confers on itself appropriateness of high pressure processing. Graphene could therefore be applied as an excellent reinforcement to ceramic materials. Recent studies on graphene-nanoplate reinforced composites like poly lactic acid [8], ultra-high-molecular-weight polyethylene [9], silicon nitride [10] and aluminum [11] already shed light on enhanced mechanical or biological properties. Incorporation of graphene nanosheet (GN) into HA could be a promising option for enhancing the biological properties of HA for biomedical applications and significantly enhanced strength has been previously revealed for HA–GN composites [12]. Biomedical application has been one of the exciting opportunities of graphene that inspired extensive explorations [13,14]. Of particular interests are graphene-based nanomaterials and their exciting biological performances [15,16]. In the light of available scientific evidences suggesting its biological performances, graphene might potentially be a good candidate for HA-based composites for biomedical applications. Compared to the conventional ceramic matrix composites reinforced by one-dimensional carbon materials such as carbon fibers, carbon nanotubes or ceramic whiskers [17–19], the further significantly enhanced fracture property of graphene-containing composites reported in recent years was ascribed to strong interfacial bonding as a result of mechanical interlocking between graphene and the matrix due to the nanoscale roughness of the platelets [6,20]. Our results have shown that the predominate toughening mechanisms for HA–GN nanocomposites are fine grain strengthening, graphene flakes pull-out, microcrack

* Corresponding author.
E-mail address: lihua@nimte.ac.cn (H. Li).

http://dx.doi.org/10.1016/j.ceramint.2016.04.038
0272-8842/

toughening, crack deflection at the HA–GN interface and crack bridging by GN [12].

It is known that high temperature heat treatment is usual for HA-based bioceramics [21]. The treatment offers the benefits of tuning phases [22], modifying topographical structures [23], and enhancing mechanical strength [24] or bioactivity [25] of the biomaterials. However, for GN-containing composites, post heat treatment might raise the problems of grain growth, decomposition, deteriorated residual stress and cracking, or structural changes of graphene at elevated temperatures [26]. To the best knowledge of the authors, behaviors of ceramic–GN composites in bulk form after heat treatment are not established yet, which would hinder potential extensive applications of GN. In this study, bulk HA–GN composites consolidated by spark plasma sintering (SPS) were heat treated for enhanced mechanical strength. Thermally induced structural damage to graphene platelets has not been seen. Direct evidence has shown that the unique presence of GN at HA grain boundaries critically inhibit HA grain growth, giving rise to promoted toughening in the composites. GN–HA interfacial adhesion and toughening mechanisms for the GN-containing composites after the heat treatment were also comprehensively elucidated.

2. Materials and methods

HA–GN nanocomposites pellets with the thickness of 5 mm have been consolidated by SPS, detailed procedure of which has been reported in detail previously [12]. To enhance the performances of the composites, post heat-treatment was performed at 800 °C with the keeping time of 2 h in a vacuum (2×10^{-2} Pa) sintering furnace (ZQL-80, China). Microstructure examination of the samples was conducted using transmission electron microscopy (TEM, FEI Tecnai F20, the Netherlands) and field emission scanning electron microscopy (FESEM, FEI Quanta FEG250, the Netherlands). Fracture properties of the pellets were measured by indentation testing made on their polished surfaces under a load of 300 gf with the loading time of 10 s using HV-1000 (Shanghai Lianer Testing Equipment Co., China). Fracture toughness (K_{IC}) of the pellets was derived from the indentation approach according to the Anstis equation [27]: $K_{Ic} = 0.016(E/H)^{1/2}(P/C^{3/2})$, where H is the measured hardness, P is the applied load, E is elastic modulus, and C is length of the crack initiated by the indentation under the load of 1000 gf. Average microhardness value for each specimen was acquired from 10 indents. Elastic modulus of the samples was determined by nanoindentation test carried out using a standard Berkovich indenter on nanomechanical test system (NANO G200, MTS, USA). The maximum indentation depth chosen for the present test was 1 μm. At least 10 indentations were made for an average value for each sample.

The experimental configuration for assessing fragmentation properties of solids has been reported by other researchers [28]. In this work, impact resistance and dynamic failure mechanism of the HA and the HA–GN composites was examined. Briefly, the SPS HA and HA–GN samples were prepared in the form of solid disks and launched with an impactor-plate facility to the impact velocity of 5.48 m/s. The diameter of the launch tube used was 10 mm. Stainless steel spheres of 9.06 ± 0.02 mm in diameter were used. The measured mass was 2.96 ± 0.02 g. Fracture surfaces of the specimens were characterized using a laser confocal microscope (ZEISS, LSM700, Germany). Both three-dimensional computer-based topographic maps and roughness parameters were acquired from the measurements.

3. Results and discussion

After the SPS consolidation, even dispersion of GN in the composites has been revealed and GN can be clearly seen at HA grain boundaries (Fig. 1). It is noted that, based on the TEM characterization, the GN-containing HA compacts show finer HA grains and the increase in content of GN gives rise to further refined HA grains (Fig. 1c-1 versus b-1). Mean HA grain size in the HA–0.1 wt% GN and the HA–1.0 wt%GN compact is ~250 nm and ~150 nm respectively, while the GN-free HA sample shows the grains of ~1.5 μm. It has been realized that during the synthesis of the HA–GN nanocomposite powder, HA grains nucleate on and grow along graphene sheets [12]. SPS is essentially a high temperature processing route, regardless of the short duration offered by the approach. The graphene sheets in the SPS composites obviously inhibit the rod-like nano HA grains from growing along at least one direction, which likely accounts in part for the finer HA grains in the GN-containing SPS samples. This effect is more pronounced in the pellets with higher content of GN.

After the heat treatment at 800 °C for 2 h, it is unsurprising to note that for the pure HA sample, HA grain growth took place with rapid continuous movement of grain boundaries in a uniform manner, showing significantly enlarged grain size of over 2.5 μm (Fig. 1a-2). In contrast, however, there is less grain growth in the HA–GN samples under the same heat treatment conditions (Fig. 1b-2 and c-2). The mean HA grain size in the HA–0.1 wt%GN and HA–1.0 wt%GN composites is ~320 nm and ~200 nm respectively, suggesting the predominate role of GN as grain growth inhibitor during the high temperature annealing by pinning grains together and impeding boundary diffusion. The size increase of HA grains is mostly seen for those without intimate contact with GN. The grains located at the places where no GN is detected are much bigger (Fig. 1c-2). In fact, GN existing at HA grain boundaries forms continuous wall zones, in turn isolates HA grains from neighboring ones (Fig. 2a). Consequently, HA grain growth along at least one direction can be effectively restrained, which presumably accounts for the finer HA grain sizes in the GN-containing HA composites. In the HA–GN pellets, grain growth is recognized for the grains growing at a high rate along the path where no GN is present, while the neighboring grains are consumed (Fig. 2a). This results in the typical microstructure of the HA–GN composites with a few very large grains. In order for this phenomenon to occur, the subset of prefer-to-grow grains must possess some advantages over their competitors, for example high grain boundary energy, locally high grain boundary mobility, favorable texture or lower local second-phase density. Even though the mechanism about the above grain growth is not known yet, the GN-restrained irregular grain growth of HA can be schematically depicted (Fig. 2b). SPS processing brought about significant changes of HA grains from rod-like shape to irregular configuration. Even dispersion of GN effectively slows down or freezes the growth of HA grains, which prevails through retarding grain boundary migration. Further high temperature heat treatment results in slight growth of the HA grains staying far away from GN or irregular growth along the direction parallel to GN for the grains intimately contacting GN. GN works favorably as inhibitor preventing remarkable growth of HA grains. It is anticipated that more GN in the HA-based composites would more effectively restrict grain growth of HA during high temperature processing, which usually takes place during fabrication of bulk HA for biomedical applications. This feature should be closely related to grain-size-dependent mechanical properties of the composites.

Assessment of the properties of the heat-treated nanocomposites showed that Young's modulus values increased from 100.4 GPa for the pure HA to 110.3 GPa for the HA–0.1 wt%GN and 148.2 GPa for the HA–1.0 wt%GN pellets. After 2 h treatment at

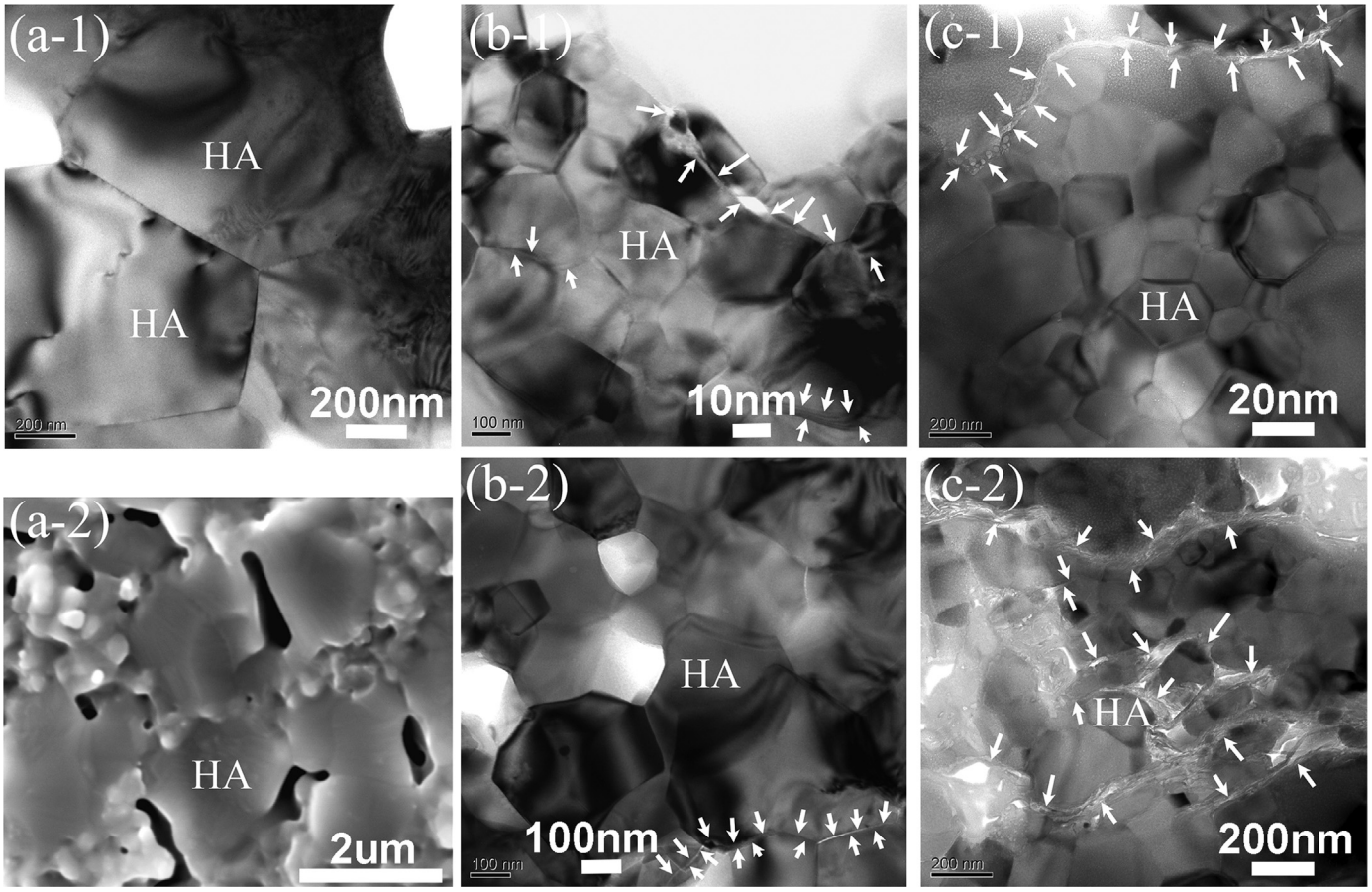

Fig. 1. Morphology of the sintered nanocomposites, (a) the pure HA pellet showing the HA grain size of ~1.5 μm in the as-sintered sample (a-1) and significantly enlarged grains of over 2.5 μm after further 800 °C annealing treatment (a-2); (b) the HA–0.1 wt%GN pellet showing restrained HA grains of ~250 nm in the as-sintered sample (b-1) and ~320 nm in the further 800 °C annealed pellet (b-2), and (c) the HA–1.0 wt%GN pellet showing significantly restrained HA grains of ~150 nm in the as-sintered sample (c-1) and ~200 nm in the further 800 °C annealed pellet (c-2, the GN-rich area is typically shown). The white arrows point to GN.

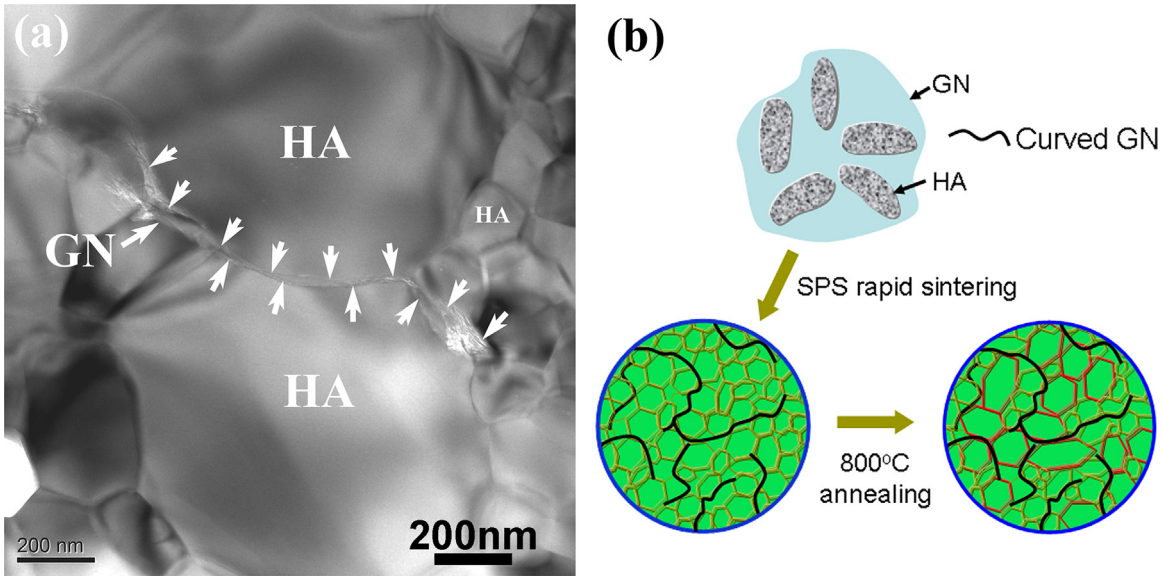

Fig. 2. Restrained HA grain growth by GN and abnormal growth of the grain along the direction parallel to GN, (a) TEM image of the HA–GN composites showing that GN is predominantly located at the HA grain boundaries, forming a serial wall zones isolating individual HA grains, and abnormal HA grain growth is seen along the direction parallel to GN, and (b) schematic depiction of the composites illustrating evolvement of the HA grains during the SPS processing and following heat treatment.

800 °C, the Young's modulus of the samples are augmented by 29.8%, 25.8% and 27.1%, respectively. In addition, increased Young's modulus values are revealed for the heat-treated samples as compared to the untreated ones, indicating improved microstructure of the nanocomposites by the heat treatment. The indentation-induced cracks are clearly seen in the pure HA pellet (Fig. 3a). In contrast, however, there is less cracking or even no cracks in the treated HA–GN samples under the same load

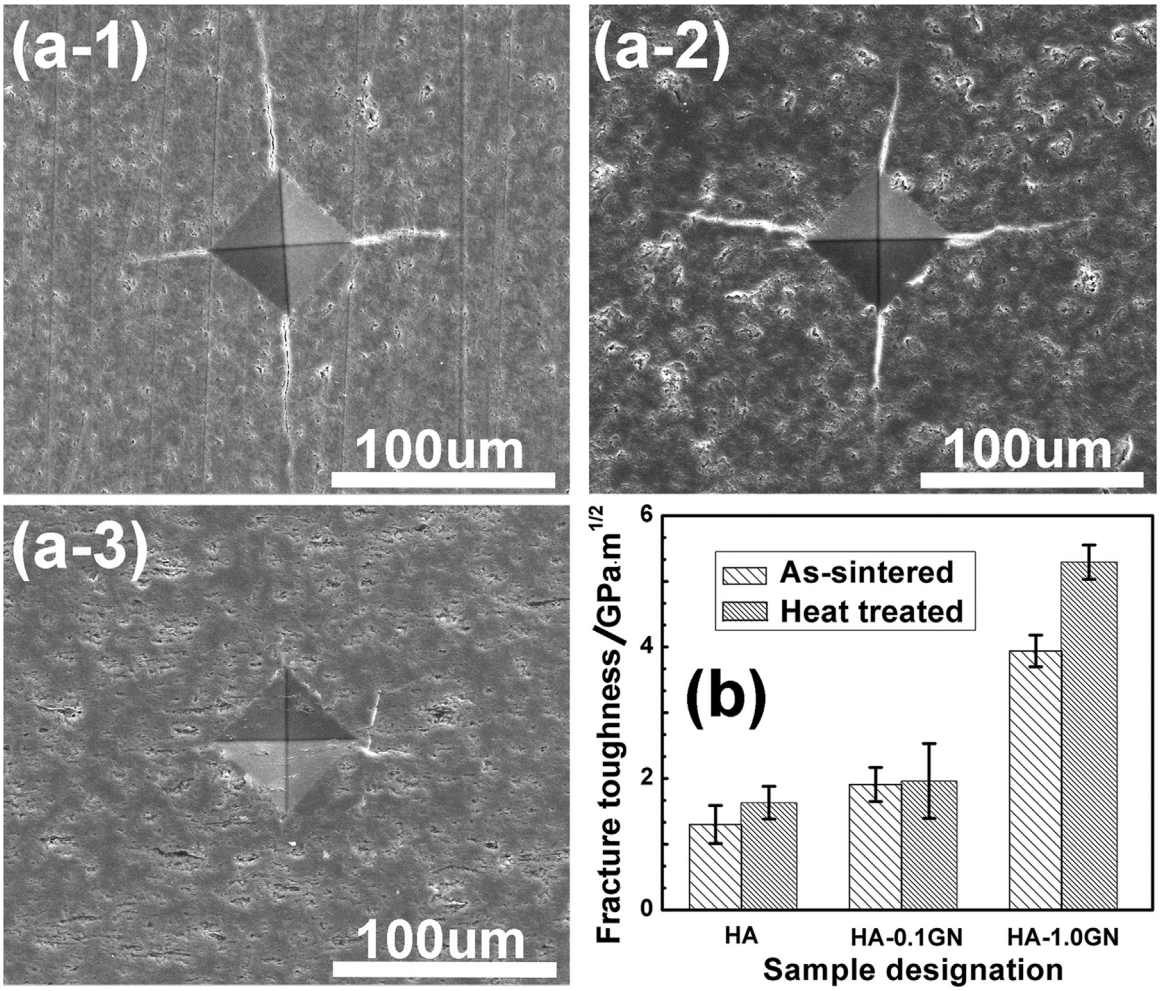

Fig. 3. SEM images of the samples showing indentation-induced craters and cracks, (a-1 and a-2): the pure HA, (b-1 and b-2): the HA–0.1 wt%GN nanocomposites, and (c-1 and c-2): the HA–1.0 wt%GN nanocomposites, – 1: as-sintered, – 2: after the 800 °C heat treatment, and (d): fracture toughness values of the pellets.

conditions (Fig. 3b and c), suggesting remarkable enhanced effect by GN on the fracture properties. The heat treatment improves the fracturing behavior of all the samples (Fig. 3a-2 versus a-1, b-2 versus b-1, c-2 versus c-1). Consistently, fracture toughness values of the GN-containing samples are higher than the pure HA sample (Fig. 3d). The post-SPS heat treatment results in marked improvement in fracture toughness. It was established that fracture pertains to capability of energy absorption [29,30], enhanced energy absorption during crack propagation gives rise to increased fracture toughness. Decrease in the size of HA grains multiplies grain boundaries. As a result, the capability of energy storing would be enhanced, which in turn prohibits advancement of cracking [31].

Biomaterials applied for hard tissue replacement in clinical surgery are usually subjected to impact loading. Impact energy mitigation is essentially required for the biomaterials. It is established that the total energy input to implant system during low-velocity loading is dissipated via total energy absorption by the implant, which is represented by damage initiation, damage propagation, sound, heat, kinetic energy of flying particles [32]. Roughness of fractured surface could be used for predicting fracture energy absorption [32]. In this work, assessment of the resistance of the heat-treated HA–GN nanocomposites to impact loading was made using an impactor-plate testing facility, which is schematically shown in Fig. 4a. The plate samples were hit by stainless steel pellet and experienced failure and dynamic fragmentation due to the impulsive loading. Evaluation of the roughness of the impact-induced fracture surfaces was made based on measuring their three-dimensional (3D) profiles. During the impacting, the pellets suffer sustain damage from surface cracks and plastic deformation at multiple collisions. The extent of surface damage at impact area is noticeably larger for HA samples (Fig. 4b) than that for the HA–GN samples (Fig. 4c and d). The pure HA pellet exhibits obvious brittle fracture, while the GN-containing composites show remarkable volumetric and shear deformations. This further indicates enhanced fracture properties of HA by addition of GN.

Areal roughness RSa of the fractured surfaces exhibits the average value of 1.983 μm, 2.213 μm, and 3.390 μm for the HA, the HA–0.1%GN, and the HA–1.0%GN pellets, respectively (Figs. 5 and S1 in the Supplemental data). Taking into account the higher fracture toughness of the GN-containing HA, these suggest that the tougher pellets exhibit rougher fractured surface. In addition, the fractured surface of the HA–GN compact shows clear pullout of GN, which is homogeneously dispersed in HA matrix (Fig. 5a). GN outcrop of 2–4 μm significantly enhanced the surface roughness (Fig. 5b). Trace of pullout of graphene flakes with cavities being left over can be clearly seen. Retained GN can also be seen on the fractured surface (inset in Fig. 5c). Griffith states that brittle fracture occurs when the released strain energy is greater than the fracture energy required to create new fracture surfaces. Consequently a more tortuous fractured surface indicates greater fracture energy absorption during crack propagation [33].

For fracture failure of the HA–GN nanocomposites, the energy

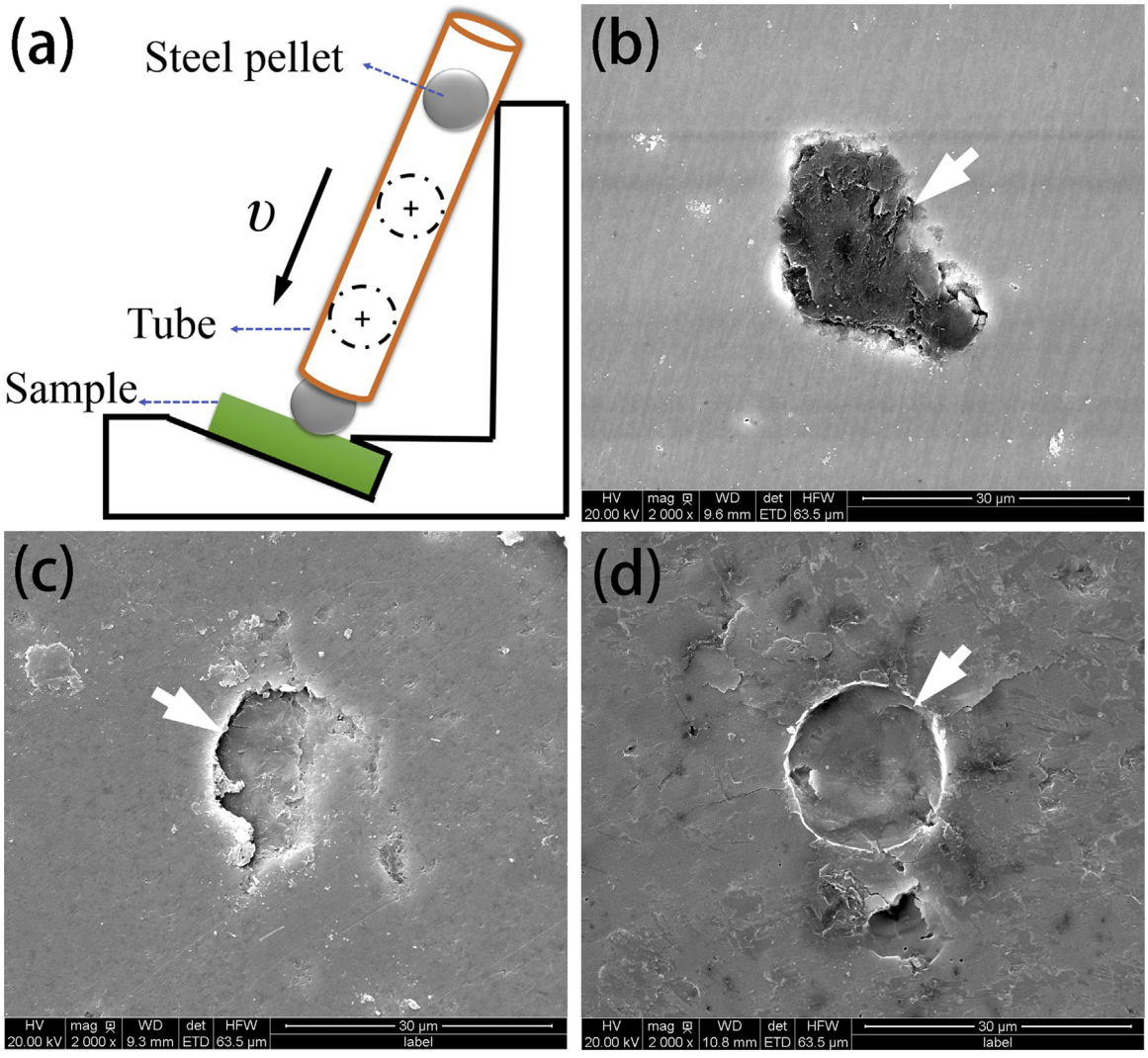

Fig. 4. Schematic depiction illustrating the impact loading testing for the samples (a), and topographical SEM images showing the impact-induced surface failure features of the pure HA pellet (b), the HA–0.1 wt%GN pellet (c), and the HA–1.0 wt%GN pellet (d). The white arrow points to impact-induced crater.

of pull-out of GN from HA matrix plays important roles. In fact, pull-out of GN has been recognized as the major failure regime for the heat-treated samples (Fig. 5d). The pull-out energy is largely dependent on intra-layer covalent bond energy of adjacent GN and interfacial shear strength between HA and GN. In theory, based on bare van der Waals or π-orbital, interaction between two neighboring graphene layers in graphite leads to an ultra-low shear strength in the order of megapascals [34]. Taking into account the intra-layer in conjunction with the high strength of carbon-carbon covalent bond, single-layered graphene possesses the strength of ~200 GPa [35]. Meanwhile, randomly-shaped graphene sheets can create additional mechanical interlocking and in turn accomplish anchoring effect at the interfaces. Close views of the structure by HRTEM already show dense interfaces between GN and HA grains in the composites (Fig. 6). Fourier transform (FFT, Fig. 6C) and inverse-FFT (IFFT, Fig. 6D) analyses of the HRTEM images acquired at the HA–GN interfaces verified GN and HA. HA grains and GN are identified by the lattice spacing of 0.272 nm for the (300) plane of HA and the honeycomb structure respectively (Fig. 6B). The open ends of graphene multi-sheets form relatively strong coherent interfaces with the (300) plane of HA crystals. This particular matching state between HA and GN in the composites further implies that (002) plane of HA crystal is parallel to GN walls, which is in good agreement with the crystallographic arrangement in the starting HA–GN powder [12]. In addition, surprisingly, it is noted that from the HA–GN interface to graphene surface, a gradual transition of interplanar spacing from 0.272 nm to 0.216 nm is observed for the (300) plane of HA (Fig. 6A). It is known that the value of carbon lattice spacing is 0.213 nm. These nevertheless indicate that during the heat treatment, HA crystals preferably align on graphene surface following the minimum atomic distance mismatch. There is no obvious evidence indicating chemical reaction between HA and GN at their interfaces. It is instead most likely that HA and GN are connected by Van der Waals bonding. It is difficult to predict the nature of the bonding between HA and GN, due mainly to structure complexity of HA crystals and the wrinkled-paper-like morphology of GN. The schematic depiction we proposed previously already illustrated the matching state of the cross-section of GN with the (002) plane of HA crystal [12]. Good interfacial bonding can be achieved by small lattice mismatch ($\delta < 0.25$) which gives rise to minor lattice strain [36]. The lattice mismatch between the (100) and (300) planes of HA crystal and cross-section of graphene walls is 0.01, which is obviously much lower than the incoherence limit of 0.25, inferring a strong bond between GN at its cross-section and HA crystal. Small measure of lattice strain resulted from the minor lattice mismatch in turn improves interfacial adhesion, which further increases fracture energy of the interfaces. The strong

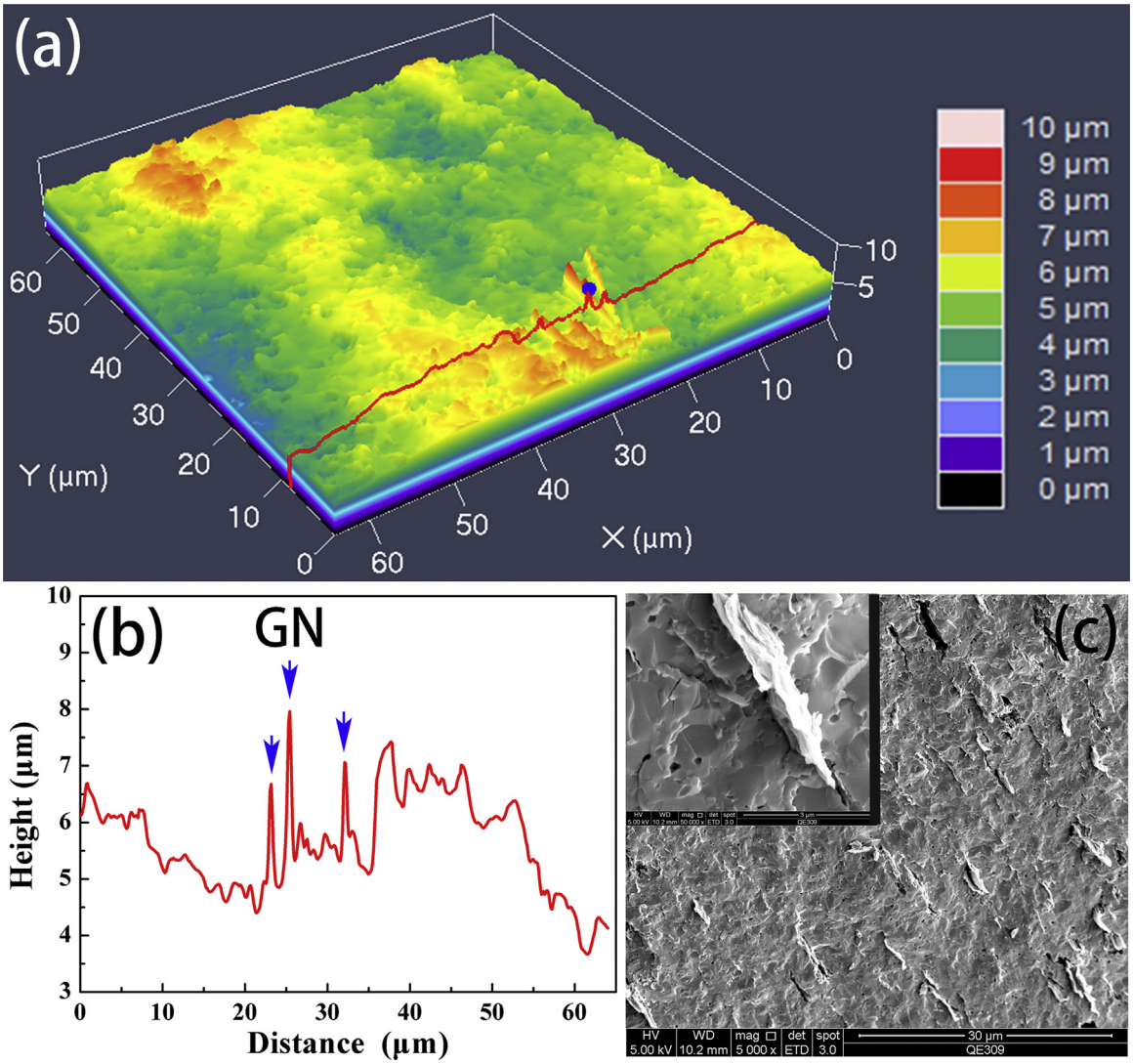

Fig. 5. (a) Typical 3D AFM topography of the fractured surface of the HA–1.0 wt%GN pellet, (b) typical vertical section profile of the fractured surface shown in (a), and (c) SEM view of impact fractured surface of the HA–1.0 wt%GN pellet (inset is enlarged view of selected area showing GN outcrop).

coherent interfaces are essentially the key for achieving competitive mechanical properties of the HA–GN composites.

The crystallographic arrangement at the HA–GN interface plays a major role in determining its strength. The energy dissipated by pull-out of GN, $E_{pull\text{-}out}$, is defined as the energy difference of the fully embedded GN from completely pull-out configuration. It can be related to the interfacial shear stress, τ, by the equations [37]:

$$E_{pull-out} = \tau \int_0^L 2(W+t)\cdot(L-x)dx = \tau(W+t)L^2, \text{ and } \tau = \frac{E_{pull-out}}{(W+t)L^2},$$

$$t = (N-1)\cdot d + h,$$

where W, L, and t are the width, length, and thickness of GN, respectively, and x is the displacement of GN, h is the effective layer (wall) thickness (~0.075 nm), d is the spacing between each graphene layer (~0.34 nm), and N is the number of graphene layers of individual GN. GN used in this study has 1–8 graphene layers, which has been determined from HRTEM characterization [12]. Since graphene is a structural analog of CNT, which is formed by tubular shaped hexagonal graphene sheet, we propose here that the interfacial shear strength (τ) between HA and graphene is approximately equal to that between HA and CNT. Cox model has been used to calculate the interfacial shear strength between HA and CNT [38], with a value of 0.3–0.35 GPa [5]. To attain debonding of graphene from HA matrix, a shear stress greater than this value has to be applied to the HA–GN interface. W, the width of GN, is 1–6 μm in this case, and L, the pull-out length of GN (2–4 μm), was measured from FESEM images. In this study, the calculated $G_{pullout}$ for single graphene sheet being departed from HA matrix is 3–40 J/m^2, much higher than the fracture energy for a monolithic HA grain, 1 J/m^2 [39]. The remarkably higher pull-out energy should be responsible for the enhanced fracture property of the HA–GN pellets.

Instant load transfer to reinforcing phases always takes place at the crack tip in composites, resulting in energy absorbing and subsequent inhibition of crack propagation. In the current HA–GN composites, single graphene sheet holds the strongest strength, while the HA–GN interface is less robust. The only disturbance to this strong interfacial bonding is the defects on graphene walls introduced possibly by the high temperature processing. These defects could be the sites for debonding of GN from HA matrix. It is therefore hypothesized here that outer layer of GN carries the maximum load transferred at HA–GN interfaces. It should be noted that in conventional fiber-based composites, higher interfacial adhesion usually leads to lower toughness, since one of the main mechanisms, fiber pull-out, is mostly suppressed [40]. However, this might not be the case for graphene-containing composites, the toughness of which is likely enhanced in the presence of

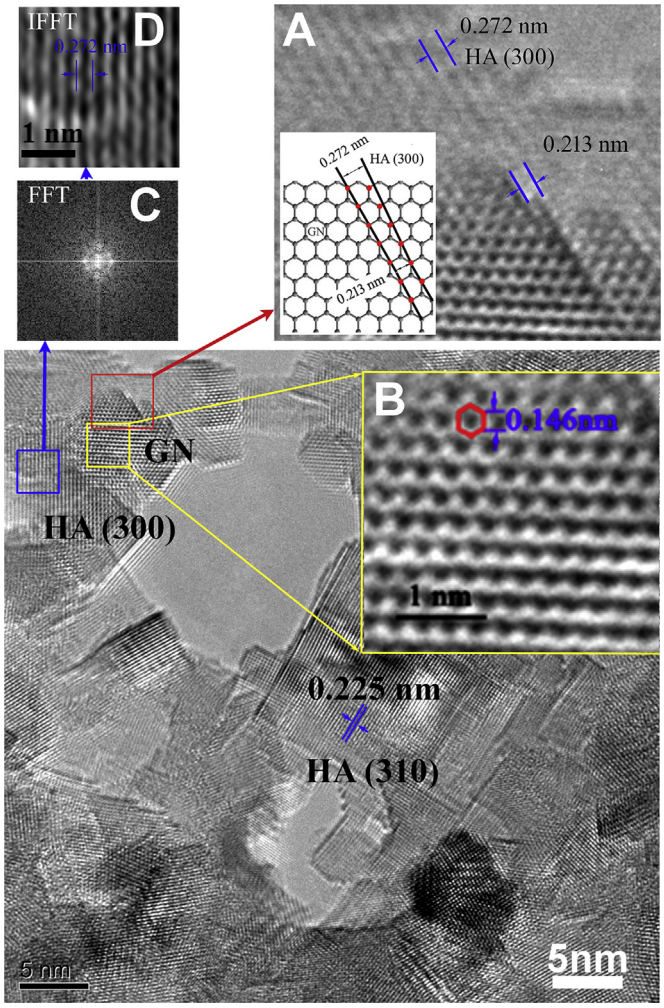

Fig. 6. HRTEM image of the heat-treated HA–1.0 wt%GN pellet showing HA–GN interfaces, FFT and IFFT analyses (C and D) further reveal the lattice spacing of GN and HA in the samples after the heat treatment. The inset image B is the enlarged view of selected area showing honeycomb structure of graphene surface, and the enlarged view A shows gradual transition of interplanar spacing for the (300) plane of HA to match the atomic arrangement of graphene.

strong interfacial bonding. Our results suggest potential applications of GN as a novel strengthening component for ceramic matrix composites.

4. Conclusions

For the HA–GN nanocomposites, through forming a serial wall zones preventing HA grains approaching each other, presence of GN at HA grain boundaries precluded effectively HA grain growth during high temperature treatment. Well-retained crystallographic arrangement at the HA–GN interfaces was revealed and is consistent with the strong bonding between HA and GN in the composites. The intact state of GN in the high temperature treated nanocomposites and the toughening brought about by GN gives clear insight into widespread high-performance structural applications of GN for ceramic-based composites.

Acknowledgments

This work was supported by National Natural Science Foundation of China (Grant # 31271017, 31500772 and 41476064), Natural Science Foundation of Ningbo (Grant # 2015A610019) and China Postdoctoral Science Foundation (Grant # 2014M561800).

Appendix A. Supplementary material

Supplementary data associated with this article can be found in the online version at http://dx.doi.org/0.1016/j.ceramint.2016.04.038.

References

[1] J. Li, B. Fartash, L. Hermansson, Hydroxyapatite-alumina composites and bone bonding, Biomaterials 16 (1995) 417–422.
[2] D. Lahiri, V. Singh, A.P. Benaduce, S. Seal, L. Kos, A. Agarwal, Boron nitride nanotube reinforced hydroxyapatite composite: mechanical and tribological performance and in-vitro biocompatibility to osteoblasts, J. Mech. Behav. Biomed. 4 (2011) 44–56.
[3] D. Singh, M. de la Cinta Lorenzo-Martin, F. Gutiérrez-Mora, J.L. Routbort, E. D. Case, Self-joining of zirconia/hydroxyapatite composites using plastic deformation process, Acta Biomater. 2 (2006) 669–675.
[4] S. Velayudhan, T.V. Anilkumar, T.V. Kumary, P.V. Mohanan, A.C. Fernandez, H. K. Varma, P. Ramesh, Biological evaluation of pliable hydroxyapatite–ethylene vinyl acetate co-polymer composites intended for cranioplasty, Acta Biomater. 1 (2005) 201–209.
[5] D. Lahiri, V. Singh, A.K. Keshri, S. Seal, A. Agarwal, Carbon nanotube toughened hydroxyapatite by spark plasma sintering: microstructural evolution and multiscale tribological properties, Carbon 48 (2010) 3103–3120.
[6] S. Stankovich, D.A. Dikin, G.H.B. Dommett, K.M. Kohlhaas, E.J. Zimney, E. A. Stach, R.D. Piner, S.T. Nguyen, R.S. Ruoff, Graphene-based composite materials, Nature 442 (2006) 282–286.
[7] L.S. Walker, V.R. Marotto, M.A. Rafiee, N. Koratkar, E.L. Corral, Toughening in graphene ceramic composites, ACS Nano 5 (2011) 3182–3190.
[8] C. Zhang, L. Wang, T. Zhai, X.C. Wang, Y. Dan, L.S. Turng, The surface grafting of graphene oxide with poly (ethylene glycol) as a reinforcement for poly (lactic acid) nanocomposite scaffolds for potential tissue engineering applications, J. Mech. Behav. Biomed. 53 (2016) 403–413.
[9] J.A. Puértolas, S.M. Kurtz, Evaluation of carbon nanotubes and graphene as reinforcements for UHMWPE-based composites in arthroplastic applications: a review, J. Mech. Behav. Biomed. 39 (2014) 129–145.
[10] L. Kvetkova, A. Duszova, P. Hvizdos, J. Dusza, P. Kun, C. Balazsi, Fracture toughness and toughening mechanisms in graphene platelet reinforced Si_3N_4 composites, Scr. Mater. 66 (2012) 793–796.
[11] J.Y. Wang, Z.Q. Li, G.L. Fan, H.H. Pan, Z.X. Chen, D. Zhang, Reinforcement with graphene nanosheets in aluminum matrix composites, Scr. Mater. 66 (2012) 594–597.
[12] Y. Liu, J. Huang, H. Li, Synthesis of hydroxyapatite-reduced graphite oxide nanocomposites for biomedical applications: oriented nucleation and epitaxial growth of hydroxyapatite, J. Mater. Chem. B 1 (2013) 1826–1834.
[13] M. Kalbacova, A. Broz, J. Kong, M. Kalbac, Graphene substrates promote adherence of human osteolbasts and mesenchymal stromal cells, Carbon 48 (2010) 4323–4329.
[14] T.R. Nayak, H. Andersen, V.S. Makam, C. Khaw, S. Bae, X. Xu, P.L.R. Ee, J.H. Ahn, B.H. Hong, G. Pastorin, B. Ozyilmaz, Graphene for controlled and accelerated osteogenic differentiation of human mesenchymal stem cells, ACS Nano 5 (2011) 4670–4678.
[15] S. Kim, S.H. Ku, S.Y. Lim, J.H. Kim, C.B. Park, Graphene-biomineral hybrid materials, Adv. Mater. 23 (2011) 2009–2014.
[16] T.H. Han, W.J. Lee, D.H. Lee, J.E. Kim, E.Y. Choi, S.O. Kim, Peptide/graphene hybrid assembly into core/shell nanowires, Adv. Mater. 22 (2010) 2060–2064.
[17] H. Hyuga, M.I. Jones, K. Hirao, Y. Yamauchi, Fabrication and mechanical properties of Si_3N_4/carbon fiber composites with aligned microstructure produced by a seeding and extrusion method, J. Am. Ceram. Soc. 87 (2004) 894–899.
[18] G.D. Zhan, J.D. Kuntz, J. Wan, A.K. Mukherjee, Single-wall carbon nanotubes as attractive toughening agents in alumina-based nanocomposites, Nat. Mater. 2 (2003) 38–42.
[19] X. Zhang, L. Xu, S. Du, W. Han, J. Han, Crack-healing behavior of zirconium diboride composite reinforced with silicon carbide whiskers, Scr. Mater. 59 (2008) 1222–1225.
[20] M.A. Rafiee, J. Rafiee, I. Srivastava, Z. Wang, H.H. Song, Z.Z. Yu, N. Koratkar, Fracture and fatigue in graphene nanocomposites, Small 6 (2010) 179–183.
[21] H. Park, S.H. Kim, Y.S. Yoon, H.B. Chae, Influence of post-heat treatment on the structure and the composition of hydroxyapatite coatings on Ti–6Al–4V deposited by using pulsed laser deposition, J. Korean Phys. Soc. 53 (2008) 3394.
[22] I.L. Denry, J.J. Peacock, J.A. Holloway, Effect of heat treatment after accelerated aging on phase transformation in 3Y-TZP, J. Biomed. Mater. Res. B Appl. Biomater. 93B (2010) 236–243.
[23] M. Gwozdzik, Z. Nitkiewicz, Topography of X39Cr13 steel surface after heat and surface treatment, Opt. Appl. 39 (2009) 853–857.
[24] W.G. Mao, J.M. Luo, C.Y. Dai, Y.G. Shen, Effect of heat treatment on deformation and mechanical properties of 8 mol% yttria-stabilized zirconia by Berkovich

nanoindentation, Appl. Surf. Sci. 338 (2015) 92–98.
[25] T. Peltola, M. Jokinen, S. Veittola, J. Simola, A. Yli-Urpo, In vitro bioactivity and structural features of mildly heat-treated sol-gel-derived silica fibers, J. Biomed. Mater. Res. 54 (2001) 579–590.
[26] Y.H. Kahng, S. Lee, W. Park, G. Jo, M. Choe, J.H. Lee, H. Yu, T. Lee, K. Lee, Thermal stability of multilayer graphene films synthesized by chemical vapor deposition and stained by metallic impurities, Nanotechnology 23 (2012) 075702.
[27] G.R. Anstis, P. Chantikul, B.R. Lawn, D.B.A. Marshall, A critical evaluation of indentation techniques for measuring fracture toughness. I. Direct crack measurements, J. Am. Ceram. Soc. 64 (1981) 533–538.
[28] D. Grady, Impact failure and fragmentation properties of tungsten carbide, Int. J. Impact Eng. 23 (1999) 301–317.
[29] L.Y. Sun, R.F. Gibson, F. Gordaninejad, J. Suhr, Energy absorption capability of nanocomposites: a review, Compos. Sci. Technol. 69 (2009) 2392–2409.
[30] J.B. Lauritzen, Hip fractures: incidence, risk factors, energy absorption, and prevention, Bone 18 (1996) S65–S75.
[31] S. Bose, S. Dasgupta, S. Tarafder, A. Bandyopadhyay, Microwave-processed nanocrystalline hydroxyapatite: simultaneous enhancement of mechanical and biological properties, Acta Biomater. 6 (2010) 3782–3790.
[32] B. Pramanik, T. Tadepalli, P.R. Mantena, Surface fractal analysis for estimating the fracture energy absorption of nanoparticle reinforced composites, Materials 5 (2012) 922–936.
[33] A.A. Griffith, The phenomenon of rupture and flow in solids, Phil. Trans. R. Soc. Lond. A 221 (1921) 163–198.
[34] M.F. Yu, B.I. Yakobson, R.S. Ruoff, Controlled sliding and pullout of nested shells in individual multiwalled carbon nanotubes, J. Phys. Chem. B 104 (2000) 8764–8767.
[35] Z. Ni, H. Bu, M. Zou, H. Yi, K. Bi, Y. Chen, Anisotropic mechanical properties of graphene sheets from molecular dynamics, Physica B 405 (2010) 1301–1306.
[36] D.A. Porter, K.E. Easterling, Phase Transformation in Metals and Alloys, third ed, CRC Press, Cheltenham, UK 2009, pp. 142–169.
[37] A. Cwirzen, K. Habermehl-Cwirzen, V. Penttala, Surface decoration of carbon nanotubes and mechanical properties of cement/CNT composites, Adv. Cem. Res. 20 (2008) 65–73.
[38] Y. Chen, K. Balani, A. Agarwal, Analytical model to evaluate interface characteristics of carbon nanotube reinforced aluminum oxide nanocomposites, Appl. Phys. Lett. 92 (2008) 011916-1–011916-3.
[39] A. Nakahira, K. Eguchi, Evaluation of microstructure and some properties of hydroxyapatite/Ti composites, J. Ceram. Process. Res. 2 (2001) 108–112.
[40] N. Lachman, H.D. Wagner, Correlation between interfacial molecular structure and mechanics in CNT/epoxy nano-composites, Compos., Part A – Appl. Sci. Manuf. 41 (2010) 1093–1098.